Université de Mons
Faculté Polytechnique – Service de Mécanique Rationnelle, Dynamique et Vibrations
31, Bld Dolez - B-7000 MONS (Belgique)
065/37 42 15 – georges.kouroussis@umons.ac.be

D. Ainalis, O. Kaufmann, J.-P. Tshibangu, O. Verlinden, G. Kouroussis, Improved analysis of ground vibrations produced by man-made sources, *Science of the Total Environment*, 616-617: 517–530, 2018.

Science of the Total Environment 616–617 (2018) 517–530

Contents lists available at ScienceDirect

Science of the Total Environment

journal homepage: www.elsevier.com/locate/scitotenv

Improved analysis of ground vibrations produced by man-made sources

Daniel Ainalis [a,*], Loïc Ducarne [a], Olivier Kaufmann [b], Jean-Pierre Tshibangu [c], Olivier Verlinden [a], Georges Kouroussis [a]

[a] Department of Theoretical Mechanics, Dynamics and Vibrations, University of Mons, Belgium
[b] Department of Geology and Applied Geology, University of Mons, Belgium
[c] Department of Mining Engineering, University of Mons, Belgium

HIGHLIGHTS

- Study of ground vibrations due to blasting, rail, and road traffic
- Comparative evaluation of dominant frequency estimation methods undertaken
- Benefits of using time-frequency distributions investigated
- Improved localised approach presented to analyse complex ground vibrations

GRAPHICAL ABSTRACT

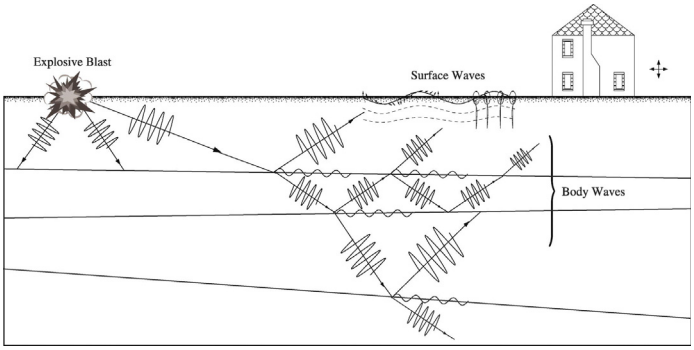

ARTICLE INFO

Article history:
Received 29 August 2017
Received in revised form 27 October 2017
Accepted 27 October 2017
Available online xxxx

Editor: P. Kassomenos

Keywords:
Ground vibrations
Blast-induced ground vibrations
Traffic-induced ground vibrations
Time-frequency analysis
Continuous wavelet transform

ABSTRACT

Man-made sources of ground vibration must be carefully monitored in urban areas in order to ensure that structural damage and discomfort to residents is prevented or minimised. The research presented in this paper provides a comparative evaluation of various methods used to analyse a series of tri-axial ground vibration measurements generated by rail, road, and explosive blasting. The first part of the study is focused on comparing various techniques to estimate the dominant frequency, including time-frequency analysis. The comparative evaluation of the various methods to estimate the dominant frequency revealed that, depending on the method used, there can be significant variation in the estimates obtained. A new and improved analysis approach using the continuous wavelet transform was also presented, using the time-frequency distribution to estimate the localised dominant frequency and peak particle velocity. The technique can be used to accurately identify the level and frequency content of a ground vibration signal as it varies with time, and identify the number of times the threshold limits of damage are exceeded.

1. Introduction

Structures and occupants in urban areas are constantly subjected to ground vibrations due to various man-made activities. These ground vibrations can induce cosmetic and structural damage and can pose a nuisance to residents. Generally speaking, the term ground vibration is used when discussing man-made activities and excludes natural phenomena such as earthquakes, and associated topography amplification (e.g. the amplification of seismic waves due to ridges, slopes, and canyons (Srbulov, 2008)). Ground vibration encompasses most man-made sources of vibration, such as construction activities, or traffic

* Corresponding author.
E-mail address: Daniel.Ainalis@umons.ac.be (D. Ainalis).

https://doi.org/10.1016/j.scitotenv.2017.10.291
0048-9697/

loading. The various complexities associated with man-made sources (and ground characteristics) results in the generation and propagation of seismic waves, each with considerably different effects.

The generated ground vibrations are dependent on not only the type of excitation but also the attenuation characteristics of the medium (Auersch and Said, 2010; Kim and Lee, 2000). There are numerous seismic waves which can be generated due to a man-made source. The first type of waves is body waves, which travel through the medium itself. There are two types of body waves; the first is the compressional P-wave which produces longitudinal particle motion. The second body wave is the transverse S-wave, which has a particle motion perpendicular to the direction of propagation. Surface waves, such as the Rayleigh wave (R-wave), and the Love wave (Q-wave), travel along the surface at slower velocities in comparison to body waves and their amplitude rapidly decreases with depth. The particle motion of the R-wave is elliptic and retrograde, isolated in a small area near the surface and horizontal to the direction of wave propagation. While R-waves are always generated in the presence of a free surface, Q-waves are only observed when there is a soft superficial layer on top of a stiffer medium. Q-waves are produced by the interference due to multiple S-waves trapped in the soft layer and the particle motion is transverse. An illustrated example of the complex propagation of body and surface waves is presented in Fig. 1.

The International Organisation for Standardisation (ISO) outlined the typical ranges of frequency and particle motions of the ground-borne vibrations generated by man-made sources under ISO 4866 (Anon, 2010), given in Table 1. From the table, it is clear that the various man-made sources can produce high-level vibrations across a similar frequency range, with the exception of blasting which can produce ground vibrations with a higher level and broader frequency range. While there are many man-made activities which generate ground vibrations, this article focuses on the analysis from three different sources: explosive blasting, road traffic, and rail traffic.

- Blast-induced ground vibrations.
  Explosives used in the construction and mining industries are of growing concern due to the increasing number of mines and quarries located near urban areas. Explosive blasting is a considerably complex problem involving the detonation of explosives, the subsequent gas expansion in each borehole, the rock fragmentation, and even crack propagation and extension (Ainalis et al., 2017b). The total explosive energy is never entirely expended in the fragmentation of the medium, and the subsequent ground vibrations generated during each blasting sequence can travel great distances (Ainalis et al., 2017b).
- Traffic-induced ground vibrations.
  Ground vibrations produced by road and rail traffic are among the most extensively studied cases. In road transport, the complex dynamic interaction between heavy vehicles and irregular pavement surfaces can generate considerable vibrations in both the vehicle and ground (Ainalis et al., 2015; Hunaidi et al., 2000; Vogiatzis, 2013). The complexity in rail transport is mainly due to the difficulty in modelling the interaction between the sequential axle loads and the track and trackbed (Carels et al., 2012; Connolly et al., 2015; Connolly et al., 2016; Kouroussis et al., 2015; Kouroussis et al., 2014).

Table 1
Typical ranges of particle motion, and frequency of ground vibrations produced by various man-made sources, from ISO 4866 (Anon, 2010).

Vibration source	Frequency range [Hz]	Particle velocity range [mm/s]	Particle acceleration range [m/s^2]
Traffic (road and rail)	1–100	0.2–50	0.02–1
Blasting	1–300	0.2–100	0.02–50
Pile driving	1–100	0.2–100	0.02–2
Outside machinery	1–100	0.2–100	0.02–1

One common issue with the analysis of the ground vibrations generated by these sources is the short duration and highly transient nature. The amplitude and frequency content of the vibration records are expected to significantly vary with time and appropriate analysis techniques are required to interpret the rapid changes in frequency and amplitude. The research presented in this paper evaluates several techniques to analyse the ground vibrations generated by various man-made sources.

2. Ground vibration analysis methods

This section presents a brief state-of-the-art on the methods used to analyse ground vibrations, along with two time-frequency analysis techniques, that monitor and assess the likelihood of structural damage occurring due to the generated ground vibrations.

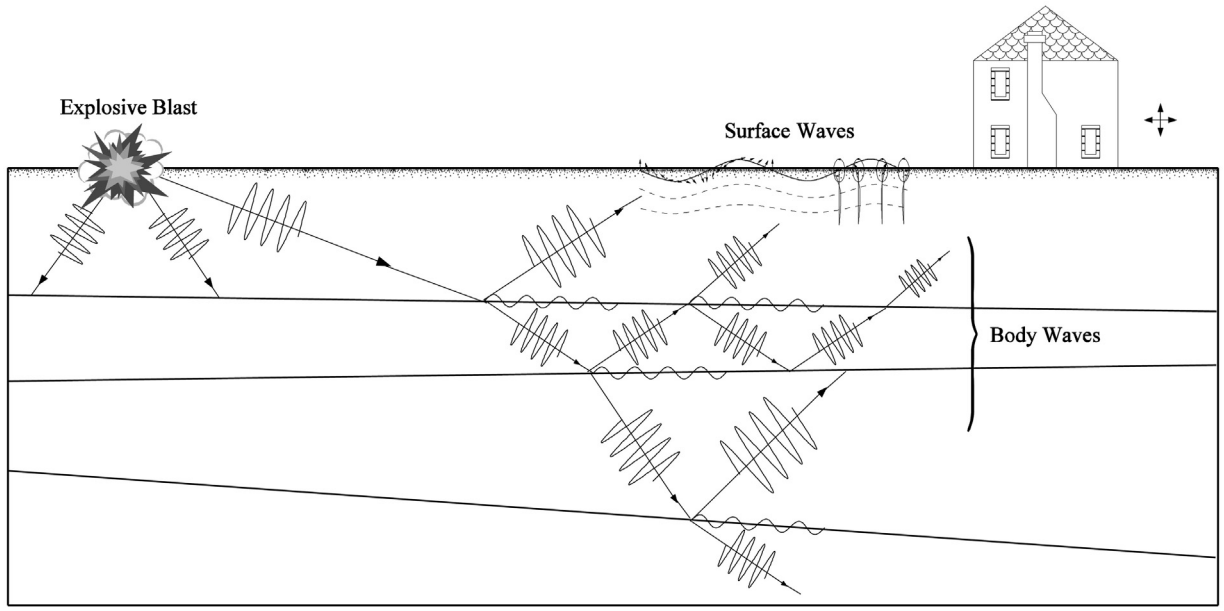

Fig. 1. Illustration of the complex propagation of the body and surface waves in the ground due to a man-made source, shown in this case due to an explosive blast.

2.1. Standard monitoring and analysis approach

There is no clear consensus on a single ground vibration analysis approach for predicting structural damage. Several organisations have published standards related to ground vibrations and its influence on humans and structures. Many of the standards listed below are based on the large-scale study on structural damage due to blast-induced ground vibrations undertaken by Siskind et al. (1980), produced for the United States Bureau of Mines (USBM). The most common standards include:

- The international standard ISO 4866 does not specifically outline a method for evaluation of vibration and structural damage, instead referring to DIN 4150-3 (Anon, 2010).
- Germany and other European countries use the German standard DIN 4150-3 (Anon, 1999).
- The United Kingdom uses standard BS 7385-1 (Anon, 1993).
- Australia uses standard AS 2187.2, limited to ground vibrations due to explosive blasts (Anon, 2006).
- In the United States of America, the Office of Surface Mining Reclamation and Enforcement published OSM Blasting Performance Standard 30, limited to blast-induced vibrations (Anon, 1983).

The standards all stipulate that the ground vibration is measured in three mutually perpendicular axes (i.e. vertical, longitudinal, and lateral). There are two key indicators used to analyse ground vibrations; the Peak Particle Velocity (PPV), and the dominant frequency. These two values are both used to assist in the prediction of the occurrence of damage (cosmetic and/or structural) using what is commonly known as the Z-Curve. While several variations of the Z-Curve exist and are available in most of the aforementioned standards, they will not be discussed further in this paper.

2.1.1. Peak particle velocity estimation

The PPV has long been the principal indicator for monitoring and evaluating ground vibrations, with several studies linking threshold PPV values with cosmetic and structural damage (e.g. (Siskind et al., 1980)). The PPV is determined by identifying the maximum absolute instantaneous velocity value of the measured time history. Generally, the PPV is calculated for each of the three measured vibration components, and only the maximum value is used. In some cases, the PPV can also be described as a three-dimensional vector, combining the instantaneous values of all three measured components. As discussed previously, the PPV alone is not sufficient and is combined with the dominant frequency of the ground vibration.

2.1.2. Dominant frequency estimation

The estimation of the dominant frequency is not as straightforward as it may seem at first. For example, standard BS 7385-2 states that the method of estimation of the dominant frequency depends on whether the ground vibrations are “simple or complex in character” (Anon, 1993). The different approaches which can be used to estimate the dominant frequency broadly fall into the following three methods:

- Zero-crossing frequency of the PPV amplitude peak.
  Use the time between the zero-crossings on either side of the PPV to estimate the dominant frequency. This is a common method for estimating the dominant frequency and can be found in many commercial data analysis software packages.
- Dominant frequency of the entire vibration time history.
  Compute the frequency spectrum from the entire time history of the vibration record, from which the dominant frequency is identified as the maximum.
- Frequency of maximum PPV amplitude peak.
  Perform a time-frequency analysis and identify the dominant frequency at the time of the PPV. This method requires an experienced user to perform the analysis and interpret the results.

The zero-crossing algorithm is a poor analysis method, taking an overly simplistic approximation of the measured ground vibrations. Computing the dominant frequency across the entire signal offers no localised information to link the dominant frequency with the level of the ground vibrations generated. Performing a time-frequency analysis can be useful to localise the frequency and greatest level of damage, however, this requires an experienced user to correctly identify and extract the relevant information. No comparative evaluation of these three methods on the analysis of ground vibrations has been undertaken, and it is of great interest to compare the localised dominant frequency when the PPV is reached, the overall dominant frequency, and the zero-crossing approach.

2.2. Time-frequency analysis methods

Two time-frequency analysis techniques used to analyse the various ground vibrations records are discussed in this section.

2.2.1. Short Time Fourier Transform

The Short-Time Fourier Transform (STFT), presented in Eq. (1), is a widely used method for the analysis of nonstationary vibration data. On the contrary to the Fourier transform, the STFT decomposes a time history signal $x(t)$ into a series of equally-sized windowed sections and computes the time-frequency distribution.

$$STFT(f,\tau) = \int_{-\infty}^{\infty} x(t)w(t-\tau)\ \exp(-j2\pi ft)dt \tag{1}$$

where f is frequency, t is time, and w is the window function.

However, the principal limitation of the STFT is that it conforms to Heisenberg's uncertainty principle, shown in Eq. (2), which limits the method's ability to provide a fine resolution in both frequency and time. From the equation, if the user requires a fine frequency resolution, then the STFT window size must be proportionally greater. Depending on the resolution (and lowest frequency) required, the user can be limited in obtaining localised frequency information in time, and therefore unable to detect abrupt changes in vibration records. Since the STFT has been in widespread use for decades, no detailed discussion on its implementation is presented. For further information, see (Cohen, 1995).

$$\delta t = \frac{1}{\Delta f} \tag{2}$$

where δt is the sub-record length (time between estimates), and Δf is the frequency resolution.

2.2.2. Continuous wavelet transform

The wavelet transform has been the subject of research for a considerable period of time, and one significant advantage it possesses over the STFT is its ability to overcome the temporal-frequency limitation. There are two distinct implementations of the wavelet transform: the discrete wavelet transform (DWT), and the continuous wavelet transform (CWT), with each better-suited for different applications. For example, the DWT is commonly used for signal and image de-noising and compression due to its ability to represent a signal (or image) with fewer coefficients. On the other hand, the CWT allows for fine-scale analysis and allows the user to set scales for each octave, enabling control over the scale resolution. The CWT is used in this paper to analyse the various ground vibrations produced by various man-made

sources. The wavelet transform of a signal $x(t)$ is defined in Eq. (3).

$$W(a,b) = \frac{1}{\sqrt{a}} \int_{-\infty}^{\infty} x(t)\psi * \left(\frac{t-b}{a}\right) dt \tag{3}$$

where $\psi(t)$ is the mother wavelet, a is the dilation factor, and b is the translation factor.

The dilation parameter (a) is used to scale the mother wavelet by stretching and shrinking it in time. A large dilation factor stretches the mother wavelet in time, and as expected corresponds to slowly varying signal changes (i.e. low frequencies). Conversely, a small dilation factor shrinks the mother wavelet and is able to detect abrupt signal changes (i.e. high frequencies). The translation parameter (b) defines how the wavelet is moved along the length of the signal, detecting any changes at the localised time where the wavelet is centred. The ability to shift and scale the mother wavelet using the dilation and translation factors is what allows the CWT to achieve a good time-frequency resolution.

It should be noted, however, that the CWT computes the scale-dependent structure of a signal as it varies with time. The scale-dependent structure has a relationship to instantaneous frequency, enabling the CWT to be used for time-frequency analysis (Sadowsky, 1996). Therefore, the appropriate selection of scales is important to obtain relevant frequency range and resolution for analysis, and this is achieved through the setting of octaves and voices. The number of octaves N_{oct} establishes the frequency range, while the voices per octave N_{voi} determines the resolution, or number of scales across each octave. While there is no exact relationship to convert scales to frequency, a close approximation to determine the pseudo-frequency F_a can be used, as shown in Eq. (4).

$$F_a = \frac{F_c}{a \cdot dt} \tag{4}$$

where F_c is the wavelet's centre frequency, a is the dilation factor, and dt is the sampling period.

Another advantage of the wavelet transform over the STFT (and, hence, the FT) is the multitude of wavelets available for use. Throughout the years, numerous mother wavelets have been developed and used for a variety of applications. The choice of mother wavelet for analysis depends on a number of factors, but the general rule is to use a wavelet which has the greatest similarity to the desired features to be extracted from the data (Randall, 2011). To demonstrate the different time-frequency relationships of the three approaches (time-scale for the CWT), a conceptual illustration is presented in Fig. 2. From the figure, it is important to note the multiresolution analysis of CWT, which allows the transform to overcome the traditional time-frequency limitations through the dilation and translation of the mother wavelet.

3. Experimental analysis of ground vibration records

This section presents a comparative evaluation of the various techniques used to analyse man-made ground vibrations. A brief note on the implementation and parameter selection of the three analysis techniques is also presented.

3.1. Parameter selection, implementation, and analysis details

This section outlines the parameter selection and any specific implementation details of the three analysis techniques used to analyse the man-made ground vibrations.

3.1.1. DIN 4150/Fourier transform approach

The current standard analysis approach involves the estimation of two parameters; the PPV, and the dominant frequency. The PPV is straightforward to calculate, and will not be discussed further. However, as previously stated, there are several methods which can be used to compute the dominant frequency. For the standard analysis approach, the dominant frequency is calculated using the zero-crossing method (f_{ZC}), and the Fourier transform (f_{FT}).

3.1.2. Short-Time Fourier Transform parameter selection and implementation

The first consideration for the STFT is the sub-record length, dictating the time between estimates and frequency resolution of the obtained estimates. A preliminary investigation into the STFT's sub-record length for the analysis of blast-induced ground vibrations was undertaken in (Ainalis et al., 2017a). The study found the best compromise between the temporal-frequency resolutions was a sub-record length of 0.75 s ($\Delta f = 1.33$ Hz) (Ainalis et al., 2017a). A Hanning window was also applied to each window to minimise leakage. Once the time-frequency distribution has been computed, two different approaches for estimating the dominant frequency are implemented. The first approach calculates the dominant frequency at the time of the PPV within the time window (f_{STFT_PPV}), and the second approach computes the maximum overall dominant frequency from the entire time-frequency distribution (f_{STFT}).

3.1.3. Continuous wavelet transform parameter selection and implementation

There are several considerations which must be made in order to use the CWT for ground vibration analysis. The most important of these is the selection of an appropriate mother wavelet, with a multitude of mother wavelets developed throughout the years for numerous applications. The general rule for selecting a mother wavelet is to use one which has the greatest similarity to the features the user desires to extract (Randall, 2011). For establishing time-frequency distributions analytic wavelets are recommended due to their ability to separate amplitude and phase components, and they also have no negative frequency components (Mallat, 2008). The analytic Morlet wavelet is a

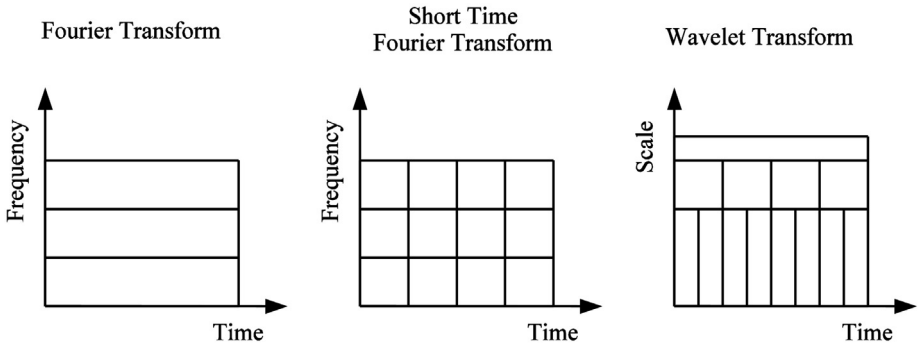

Fig. 2. Conceptual comparison of the time-frequency relationship obtained using the Fourier transform, the Short-Time Fourier Transform, and the wavelet transform.

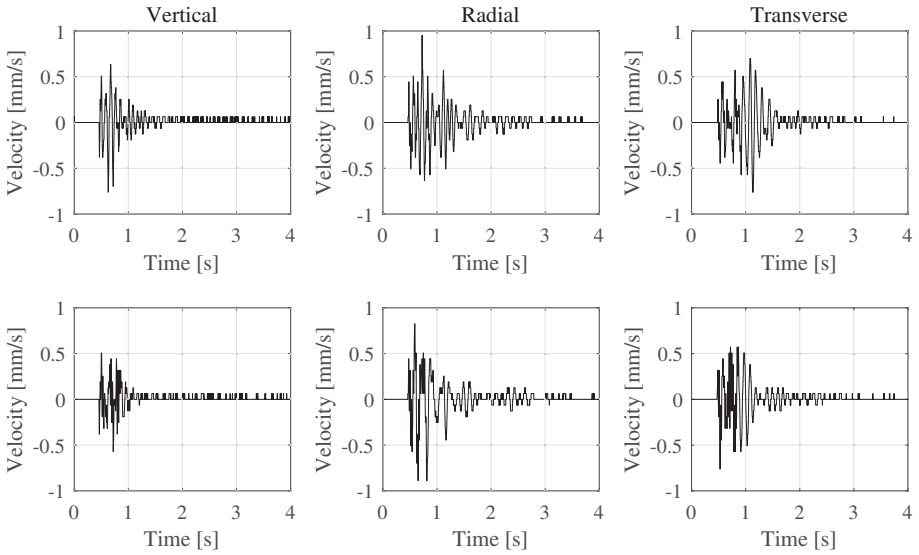

Fig. 3. Time histories of the measured tri-axial ground vibrations for dataset BL_01 (top row), and dataset BL_02 (bottom row).

complex exponential function multiplied by a Gaussian window and is suitable for time-frequency analysis since its scale can be expressed more easily in the frequency domain than other wavelets (Staszewski and Giacomin, 1997). The Morlet wavelet meets these criteria and is used in this study to analyse the various ground vibration records.

The next consideration for the implementation of the CWT is to define the range and resolution of the scales. This is achieved by setting the number of octaves, and voices per octave. The train and blast-induced ground vibration measurements were analysed using the CWT with 10 octaves (N_{oct}), each with 30 voices (N_{voi}). Due to the lower sampling rate of the ground vibration data from the passage of a truck, its analysis using the CWT has 7 octaves, with 10 voices per octave. Finally, as with the analysis using the STFT, the overall dominant frequency from the time-frequency distribution is determined (f_{CWT}), and the dominant frequency at the time of the PPV (f_{CWT_PPV}).

3.2. Blast-induced ground vibrations

The first case study is focused on the analysis of ground vibrations due to explosive blasting. In comparison to road and rail traffic, blast-induced ground vibrations have a short duration and are highly transient (Ainalis et al., 2017b). A series of blast-induced ground vibration measurements were made in the far-field using seismometers for numerous blasts undertaken at a quarry located near Tubize, Belgium. The vertical, radial, and transverse components of the ground vibration were measured at various locations around the site as part of the required monitoring procedures during the period of January 2015 to January 2016. Only two datasets were selected at random for analysis in this paper, denoted as BL_01 and BL_02, sampled at 1024 Hz for a total duration of 4.5 s. A preliminary inspection of the ground vibrations revealed that no significant energy content above 100 Hz, limiting the frequency range of the analysis to 0–100 Hz. The time histories of the blast-induced ground vibrations are presented in Fig. 3.

The DIN 4150-3 standard analysis approach is followed to compute the PPV, and also the dominant frequency using both the zero-crossing and Fourier transform methods. The overall frequency content of the analysed ground vibration data (obtained using the Fourier transform) are presented in Fig. 4. From the spectra, it is clear that there is a broad dominant contribution of frequencies between 5 and 15 Hz. In some cases, such as the transverse component of record BL_02, a smaller contribution from higher frequencies is also present.

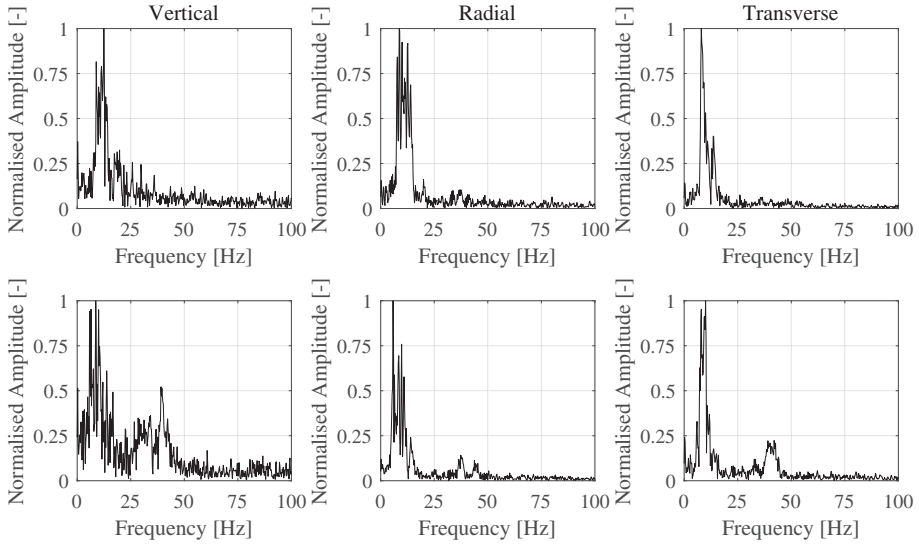

Fig. 4. Frequency content of the measured blast-induced tri-axial ground vibrations for dataset BL_01 (top row), and dataset BL_02 (bottom row).

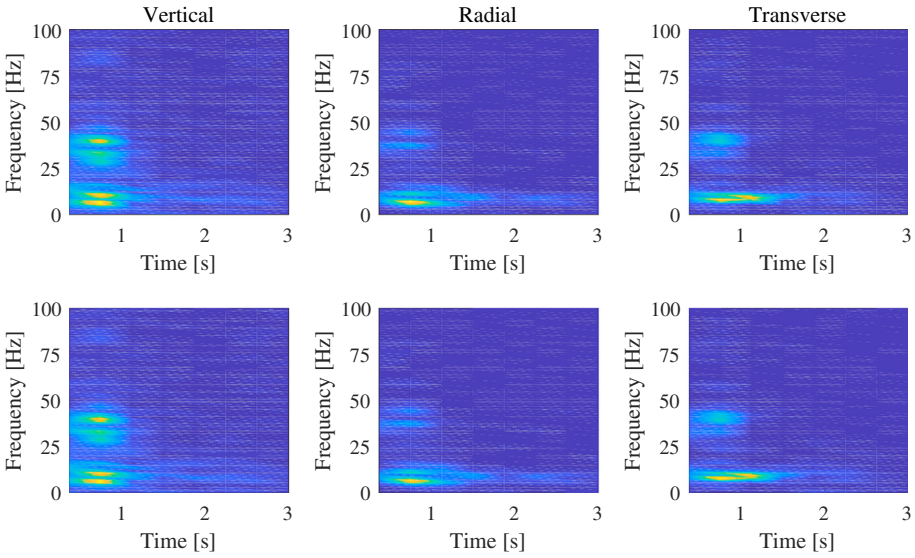

Fig. 5. Time-frequency analysis of the tri-axial blast-induced ground vibrations using the Short-Time Fourier Transform ($\delta t = 0.75$ s; $\Delta f = 1.33$ Hz), for records BL_01 (top row), and BL_02 (bottom row).

The ground vibration records were then analysed using the STFT and the CWT to compute the time-frequency distribution. The time-frequency analysis of the blast-induced ground vibration records using the STFT are given in Fig. 5, while the CWT analysis is presented in Fig. 6. Both analyses are only shown from 0 to 3 s due to the lack of significant vibration energy after this time. There is clearly a significant contribution from numerous different frequencies throughout the evolution of the signal. It is also evident that the CWT provides a far superior time-frequency distribution, able to clearly identify rapid changes in frequency content in comparison to the STFT.

The estimated dominant frequencies using the various methods, along with the overall PPV for each blast-induced ground vibration record, are summarised in Table 2 and Fig. 7. There is a general consistency of the dominant frequency estimates between the various methods within approximately 5–12 Hz, however, the zero-crossing method significantly overestimates the dominant frequency for all cases. From the two methods using the time-frequency distributions (at the PPV time, and overall), the dominant frequency estimates are fairly consistent. The only exceptions are the estimates obtained from the CWT at the time of PPV for the vertical component of BL_02, and overall for the radial component of BL_02.

3.3. Truck-induced ground vibrations

The ground vibrations induced by the passage of a heavy vehicle over a speed hump were analysed next. The ground vibration data were obtained through the use of a two-step numerical simulation. The first step involved the calculation of the dynamic loads exerted onto the pavement using a Volvo FL6 truck half-car (no roll) multibody model. The vehicle travelled over a trapezoidal obstacle that was 1.7 m long and 54 mm high at two constant speeds; 30 and 60 km/h. The dynamic loads were then inputted into a finite element ground model to simulate the ground vibration propagation. From the model, the tri-axial ground vibrations were recorded for a duration of 5 s at a distance

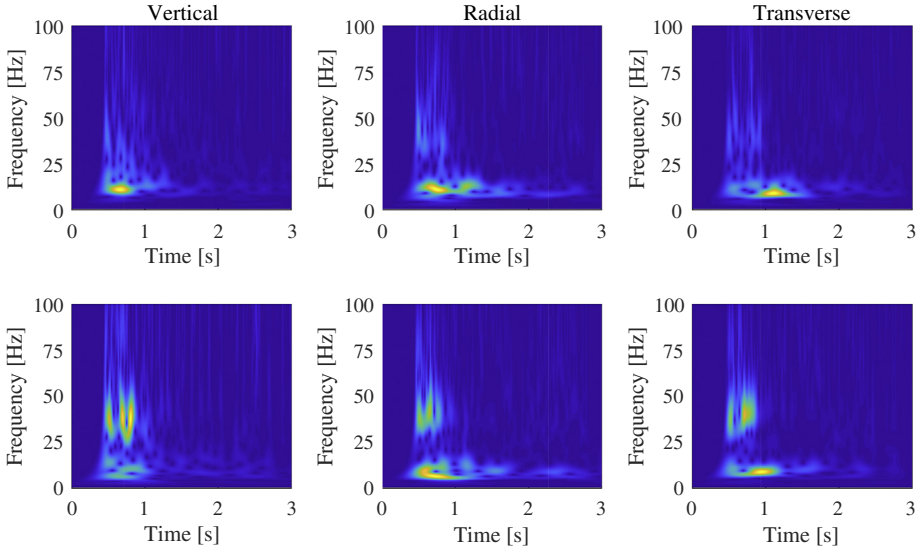

Fig. 6. Time-frequency analysis of the tri-axial blast-induced ground vibrations using the continuous wavelet transform ($N_{oct} = 10$; $N_{voi} = 30$) for records BL_01 (top row), and BL_02 (bottom row).

Table 2
Analysis of the blast-induced ground vibrations to compute the PPV, and a comparison of the various methods to estimate the dominant frequency.

Vibration record	PPV [mm/s]	Dominant frequency estimations			
		Zero-crossing f_{ZC} [Hz]	Fourier transform f_{FT} [Hz]	Short Time Fourier Transform f_{STFT_PPV}/f_{STFT} [Hz] At PPV/overall	Continuous wavelet transform f_{CWT_PPV}/f_{CWT} [Hz] At PPV/overall
RV_01					
Vertical	0.623	17.07	12.44	6.67/6.67	11.04/11.04
Radial	0.950	19.69	8.66	6.67/8.00	11.28/9.08
Transverse	0.693	19.32	8.00	9.33/6.67	9.08/6.56
RV_02					
Vertical	0.495	40.96	8.66	6.67/6.67	37.95/11.04
Radial	0.823	15.75	5.78	6.67/6.67	7.48/37.95
Transverse	0.566	18.96	10.00	8.00/8.00	8.51/8.89

of 8 m from the centre of the road, and the sampling frequency is 100 Hz. For complete details surrounding the development and implementation of the vehicle and ground models, see (Ducarne et al., 2017; Kouroussis et al., 2017). The time histories of the simulated ground vibrations due to the heavy vehicle travelling at 30 and 60 km/h over the trapezoidal obstacle are presented in Fig. 8.

First, the data were analysed according to the standard approach, where the PPV and dominant frequency are determined for each of the records. The frequency spectra of the ground vibrations are presented in Fig. 9, and the dominant frequency estimated using these spectra (Fourier transform), and the zero-crossing method.

Next, the time-frequency distributions were computed for the truck-induced ground vibrations, with the STFT analysis presented in Fig. 10, and the CWT analysis in Fig. 11. Again, it is obvious that the CWT provides a finer-scale time-frequency distribution, and the complex localised changes in the frequency content of the ground vibrations are easily identified in comparison to the STFT.

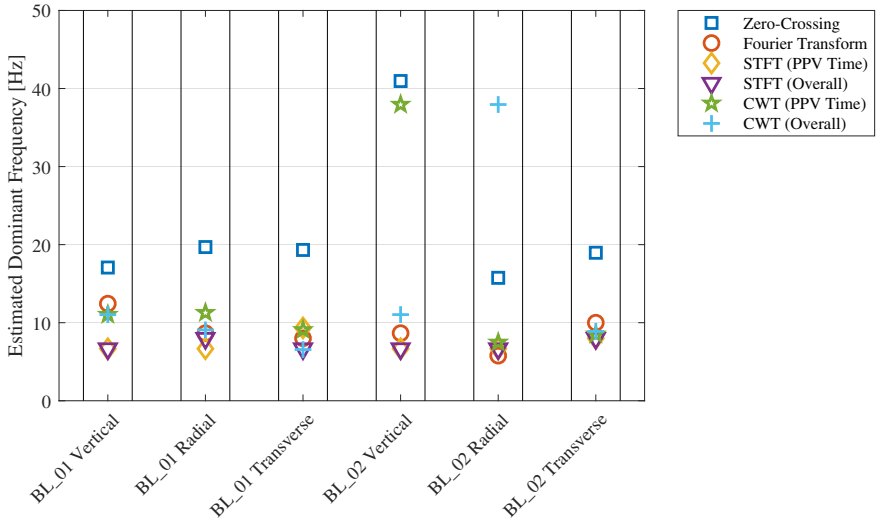

Fig. 7. Comparison of the dominant frequency estimates of the various approaches for all three components of the two blast-induced ground vibrations.

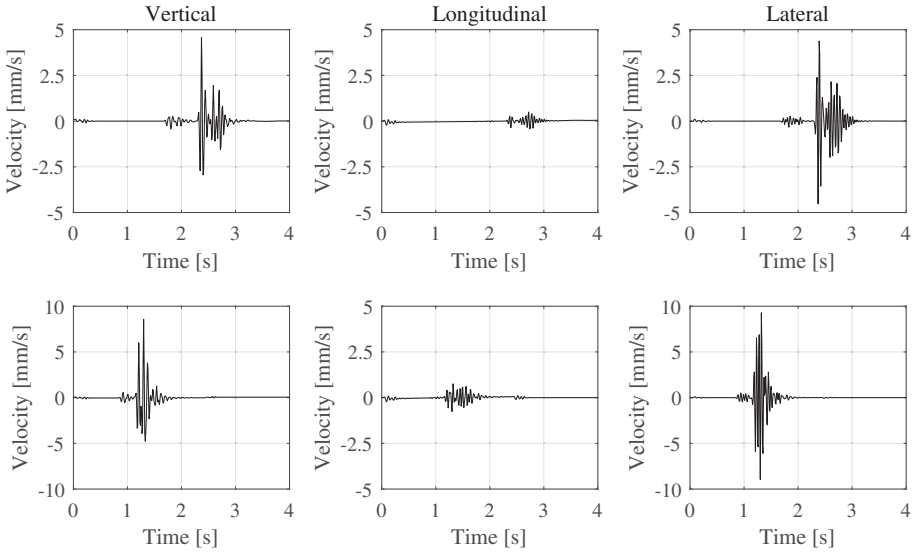

Fig. 8. Time histories of the simulated tri-axial ground vibrations (8 m from the centre of the road) due to the passage of a half-car Volvo FL6 truck travelling over a trapezoidal obstacle at a speed of: 30 km/h (RV_01, top row), and 60 km/h (RV_02, bottom row). Note the different particle velocity scales.

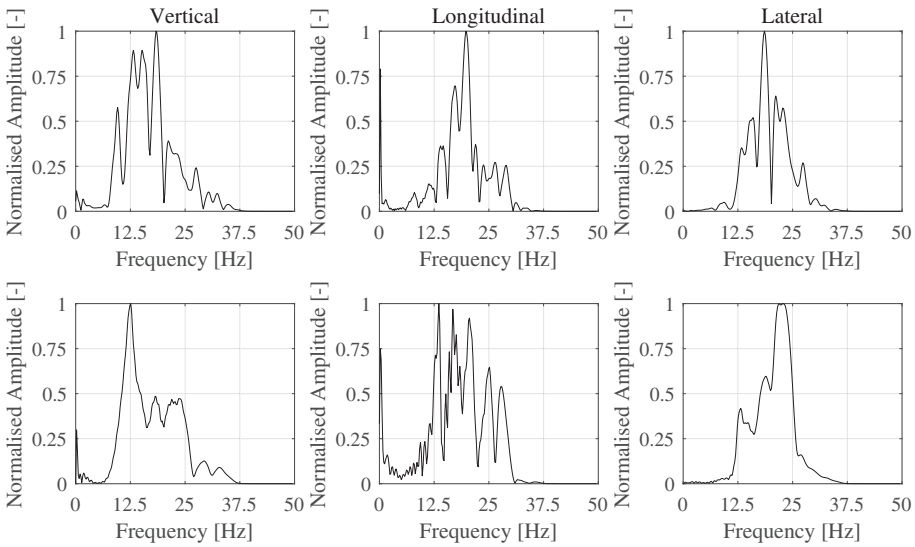

Fig. 9. Frequency content of the measured tri-axial ground vibrations (8 m from the centre of the road) produced by the passage of a Volvo FL6 tuck over a trapezoidal obstacle at 30 km/h (RV_01, top row), and 60 km/h (RV_02, bottom row).

The estimated PPV, and dominant frequencies using the various analysis methods are summarised in Table 3, along with their visual presentation in Fig. 12. As noted with the blast-induced ground vibrations, the zero-crossing method significant over- and underestimates the dominant frequency. In general, the time-frequency analysis estimates at PPV time, and overall are fairly similar to those obtained using the Fourier transform. In particular, those obtained at the PPV time are closest to the Fourier transform estimates, however, the difference to the overall estimates using the STFT and CWT are not significantly different. The biggest difference is observed for the overall dominant frequency estimates using the STFT and CWT for the vertical component of record RV_02.

3.4. Train-induced ground vibrations

A series of experimentally measured ground vibrations due to the passing of rail traffic are analysed in this section. The tri-axial ground vibration data (vertical, longitudinal, and lateral) produced by the passing of two different AM96 trains over a singular track defect was measured with a sampling frequency of 500 Hz for 15 s. The AM96 trains are commonly used by the Belgian railway operator NMBS/SNCB for InterCity and InterRegion connections, and the vehicles are known for their excellent passenger comfort. The train consists of three sets of successive carriages, the first with a motorised bogie, and the second and third are standard trailer carriages. For complete details regarding the experimental set-up and measurements, see (Kouroussis et al., 2013; Kouroussis et al., 2016). The details of the trains and ground vibration measurements for the two selected datasets are given in Table 4, and the time history of the measured tri-axial ground vibrations are presented in Fig. 13. Again, a preliminary inspection of the datasets revealed no significant energy content above 100 Hz, limiting the results to 0–100 Hz.

For all datasets, the PPV is calculated, as is the dominant frequency using the zero-crossing method and the Fourier transform. The

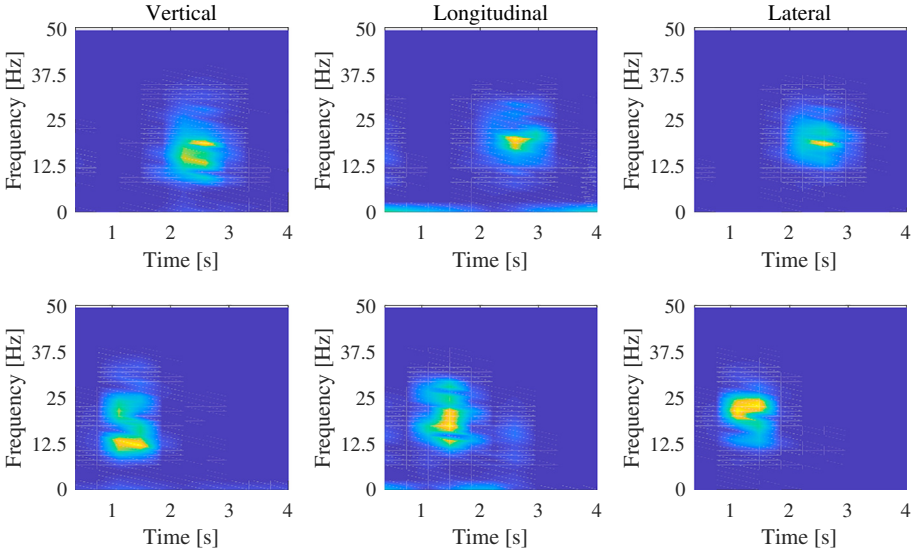

Fig. 10. Time-frequency analysis of the tri-axial truck-induced ground vibrations using the Short-Time Fourier Transform ($\delta t = 0.75$ s; $\Delta f = 1.33$ Hz) for records RV_01 (top row), and RV_02 (bottom row).

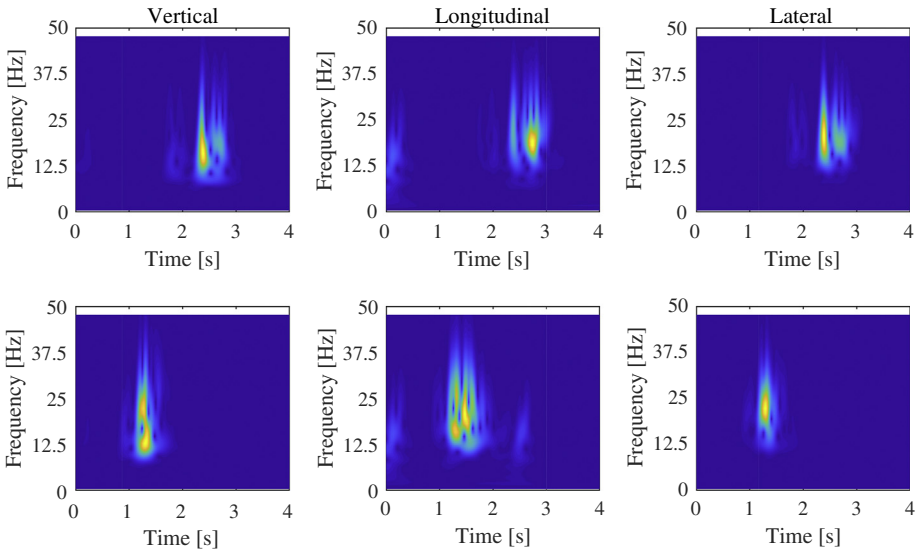

Fig. 11. Time-frequency analysis of the tri-axial truck-induced ground vibrations using the continuous wavelet transform ($N_{oct} = 7$; $N_{voi} = 10$) for records RV_01 (top row), and RV_02 (bottom row).

Table 3
Analysis of the road traffic-induced ground vibrations to compute the PPV, and a comparison of the various methods to estimate the dominant frequency.

Vibration record	PPV [mm/s]	Dominant frequency estimation			
		Zero-crossing f_{ZC} [Hz]	Fourier transform f_{FT} [Hz]	Short Time Fourier Transform f_{STFT_PPV}/f_{STFT} [Hz] At PPV/overall	Continuous wavelet transform f_{CWT_PPV}/f_{CWT} [Hz] At PPV/overall
RV_01					
Vertical	4.582	33.33	18.36	14.67/18.67	16.88/15.75
Radial	0.500	0.59	19.76	20.00/18.67	19.39/20.78
Transverse	4.382	33.33	18.56	20.00/17.33	20.78/20.78
RV_02					
Vertical	8.572	25.00	12.57	13.33/20.00	12.79/18.09
Radial	0.757	2.00	13.57	17.33/12.00	15.75/12.79
Transverse	9.281	50.00	22.75	22.67/21.33	22.27/22.27

frequency spectra of the six individual ground vibration records were computed, and are presented in Fig. 14.

Next, time-frequency analysis of the train-induced ground vibrations was undertaken using the STFT, and the CWT. First, the time-frequency distributions of the vibration records obtained by the STFT are presented in Fig. 15, while the CWT distributions are given in Fig. 16. From the established time-frequency distributions, it is clear that the train-induced ground vibrations have far more complexity in terms of the evolution of the energy content across the frequency range, and their duration is also significantly longer than both the truck- and blast-induced ground vibration records.

The results of the dominant frequency estimation using the different methods are listed in Table 5 and visually summarised in Fig. 17. Of the three different man-made sources investigated in this study, the passage of a train (with numerous axles) over a singular defect produces ground vibrations characterised by a longer duration and more complex frequency content. There is a significant variation between the dominant frequency estimates between the methods, unlike the blast- and

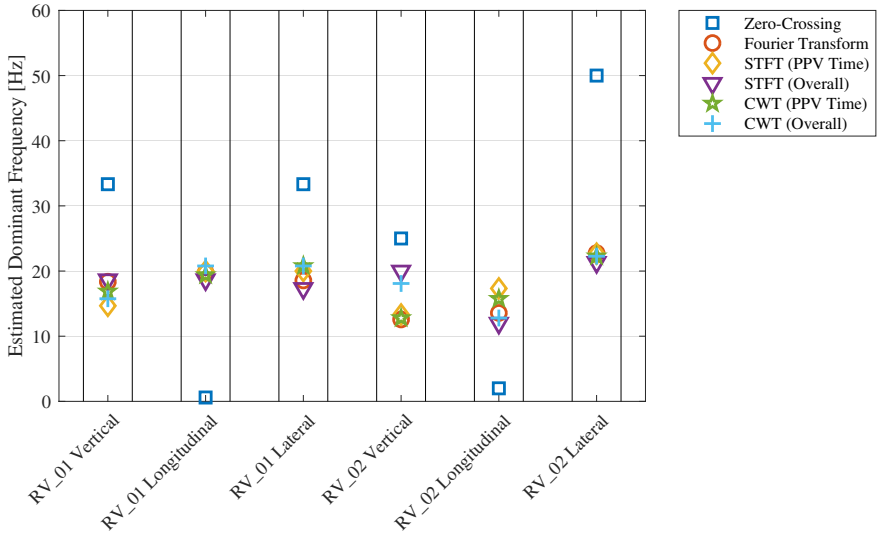

Fig. 12. Comparison of the dominant frequency estimates of the various approaches for all three components of the two truck-induced ground vibrations.

Table 4
Details of the trains used in the study and ground vibration measurement distance.

Dataset	Train type	No. of carriages	Train speed [km/h]	Distance from track [m]
TR_01	AM96	9 (3 × 3)	110	14
TR_02	AM96	6 (2 × 3)	125	14

truck-induced ground vibrations. The principal challenge associated with longer duration ground vibrations due to multiple loadings is how to determine which identified dominant frequency is the correct one and if it is linked to the PPV. The next section presents a new, improved method to analyse such complex ground vibrations.

4. Improved approach for evaluating the structural damage due to ground vibrations

This section presents an improved approach for estimating the PPV and dominant frequency using the computed time-frequency distribution. Since numerous phenomena can produce long-duration ground vibrations, particularly road and rail traffic with multiple axles, a single estimate of the PPV and dominant frequency is not sufficient for analysis and monitoring purposes. For ground vibration records which have a short duration, such as those produced by small-scale explosive blasts, there is no additional benefit to performing such detailed analysis. The following method can be used for long-duration ground vibrations to provide a useful summary of the dominant frequencies and PPVs. The example presented in the following sections is undertaken using only the CWT. While the STFT could also be used, the preceding analyses of the ground vibration records demonstrated the effectiveness of the CWT to establish a fine-scale time-frequency distribution in comparison to the STFT.

4.1. General procedure of localised analysis

The general procedure of the improved approach consists of the following three steps:

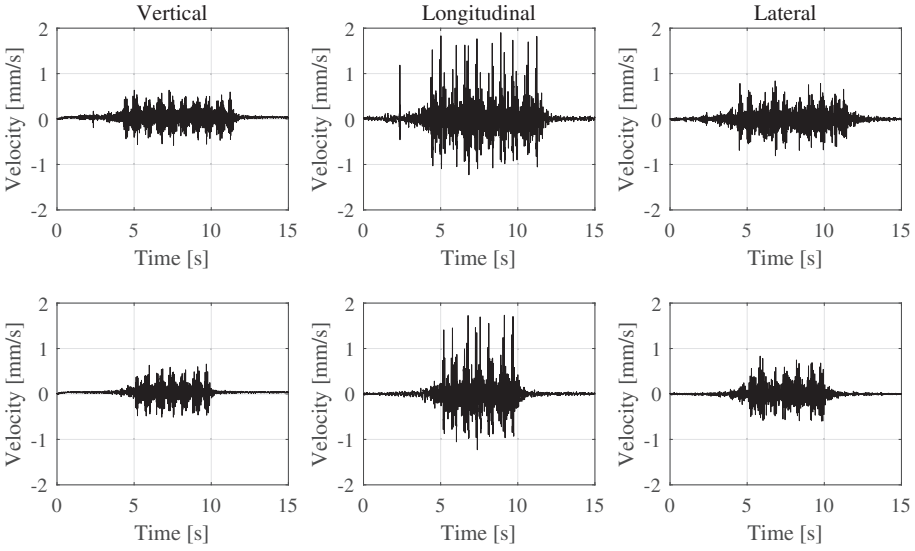

Fig. 13. Time histories of the measured tri-axial ground vibrations (14 m from the track) due to the passage of an AM96 train (3 × 3) at 110 km/h (TR_01, top row), and an AM96 train (2 × 3) at 125 km/h (TR_02, bottom row).

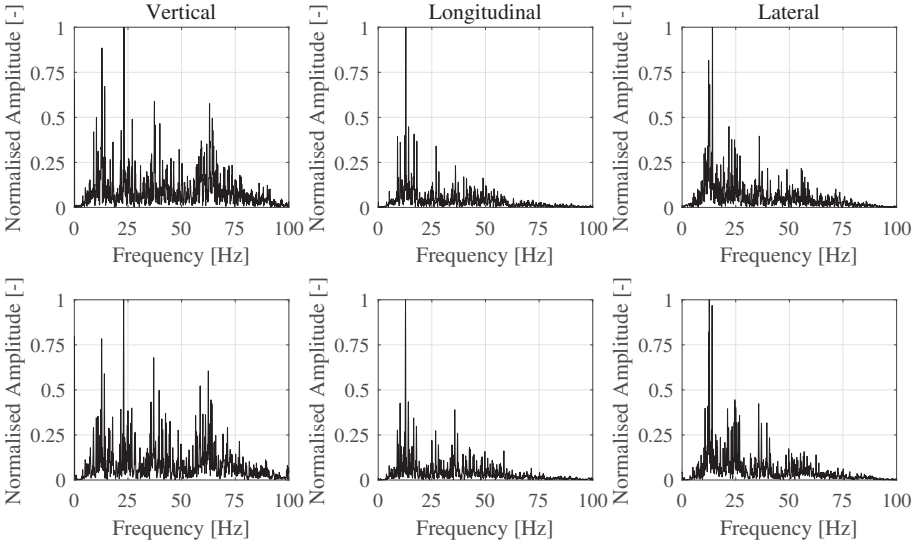

Fig. 14. Frequency content of the measured train-induced tri-axial ground vibrations (14 m from the track) produced by the passage of: an AM96 train (3 × 3) at 110 km/h (TR_01, top row), and an AM96 train (2 × 3) at 125 km/h (TR_02, bottom row).

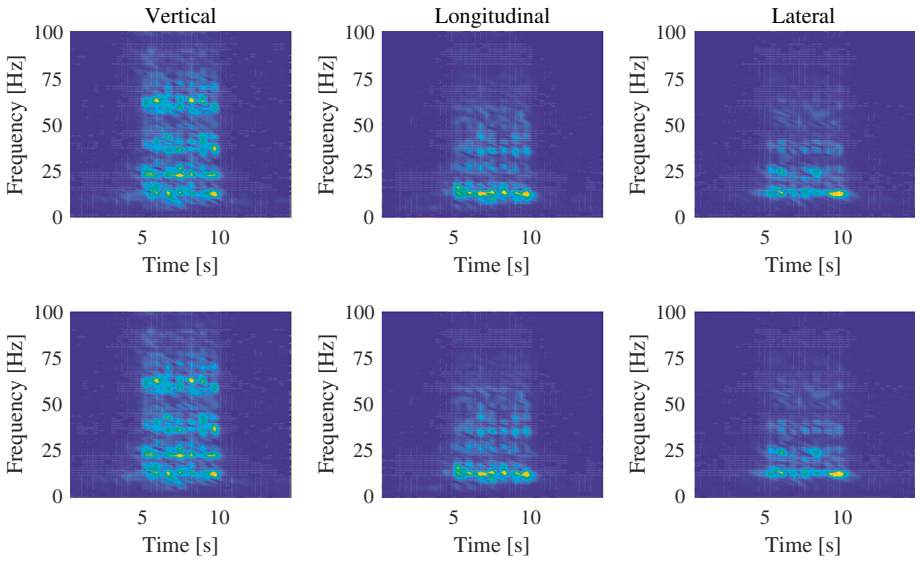

Fig. 15. Time-frequency analysis of the tri-axial train-induced ground vibrations using the Short-Time Fourier Transform ($\delta t = 0.75$ s; $\Delta f = 1.33$ Hz) for records TR_01 (top row), and TR_02 (bottom row).

1. Compute the time-frequency distribution of the measured ground vibrations (using the CWT).
   The time-frequency distribution is computed using the same implementation of the CWT as in the previous section was used, with the same mother wavelet, octaves, and voices per octave.
2. Specify a time window T_w, and for each window calculate the localised PPV and dominant frequency.
   There are two ways to select the time window to calculate the localised PPV, and dominant frequency. For example, if the STFT was used, then the time window is fixed to the sub-record length. However, since the CWT provides multiple scales (as illustrated in Fig. 2), the user is afforded more flexibility in selecting a window to calculate the localised estimates from the CWT's time-frequency distribution.
3. Sum up the results and plot them on the DIN 4150-3 Z-Curve.
   Having obtained a number of localised PPV and dominant frequency estimates, plot all the data points on the DIN 4150-3 Z-Curve to assess the likelihood of structural damage occurring.

Next, example analyses using the improved (localised) approach for monitoring ground vibrations due to man-made sources is presented and compared with the current analysis procedure.

4.2. Example analyses using the localised analysis approach

Some analysis examples of man-made ground vibrations using the improved ground vibration analysis approach is presented in this section. To illustrate the method, the tri-axial components of the ground vibration records TR_01, RV_01, and BL_01 are analysed using the improved approach, and compared to the standard analysis approach of computing the overall PPV, and the dominant frequency using the Fourier transform. For the localised estimates, the duration of the window within which each estimate is made is set to $T_w = 0.5$ s. The resulting estimates of the localised PPV and dominant frequency are then compared with the DIN 4150-3 Z-Curves to assess whether structural damage is likely to occur. The resulting analysis using the localised

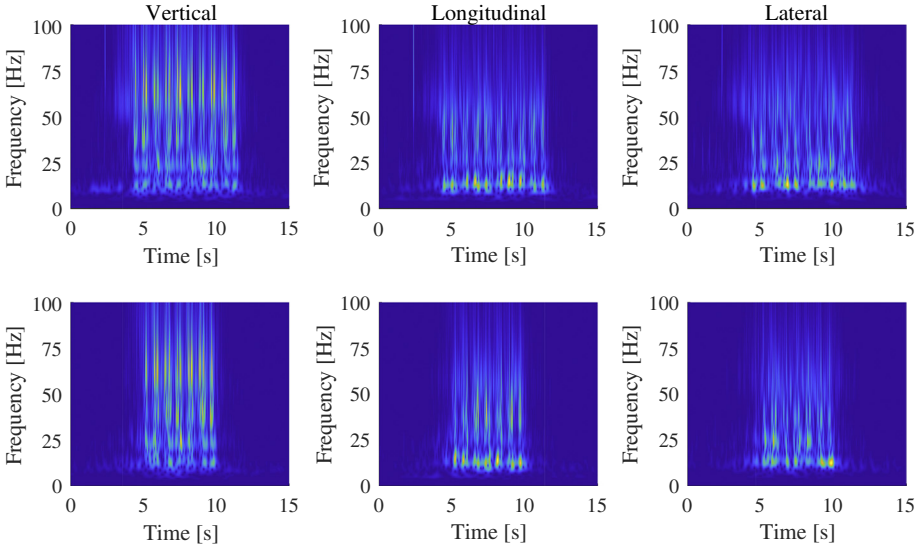

Fig. 16. Time-frequency analysis of the tri-axial train-induced ground vibrations using the continuous wavelet transform ($N_{oct} = 10$; $N_{voi} = 30$) for records TR_01 (top row), and TR_02 (bottom row).

Table 5
Analysis of the train-induced ground vibrations to compute the PPV, and a comparison of the various methods to estimate the dominant frequency.

Vibration record	PPV [mm/s]	Dominant frequency estimation			
		Zero-crossing f_{ZC} [Hz]	Fourier transform f_{FT} [Hz]	Short Time Fourier transform f_{STFT_PPV}/f_{STFT} [Hz] At PPV/overall	Continuous wavelet transform f_{CWT_PPV}/f_{CWT} [Hz] At PPV/overall
RV_01					
Vertical	0.635	45.45	23.13	26.67/62.67	68.56/63.97
Radial	1.901	45.45	12.87	13.33/12.00	14.41/13.45
Transverse	0.839	33.33	14.13	13.33/13.33	13.45/13.92
RV_02					
Vertical	0.658	50.00	23.00	12.00/13.33	66.22/14.41
Radial	1.732	26.32	12.73	13.33/62.67	11.71/66.22
Transverse	0.832	45.45	12.67	13.33/12.00	13.45/12.55

approach, and the standard analysis approach of the train-induced ground vibrations are presented in Fig. 18, while the analysis results of the truck-induced ground vibrations are presented in Fig. 19. The analysis of the blast-induced ground vibrations are presented in Fig. 20. It should be noted that the vertical axis of the Z-Curve has been set to logarithmic scale in order to clearly show all localised estimates.

For all the analysed vibration records, the PPV and dominant frequency estimate obtained by the standard approach (Fourier transform to estimate the dominant frequency) are fairly consistent to the maximum obtained by the improved localised approach. Interestingly, the analysis of the vertical component of TR_01 shows a significantly different dominant frequency linked to the maximum PPV. The localised analysis reveals that the dominant frequency at the time of the PPV is much higher than the overall dominant frequency. For the vertical and lateral components of vibration record RV_01, both the standard analysis approach and the improved localised approach indicate that the ground vibrations generated could cause structural damage to buildings considered to be 'sensitive' according to the DIN 4150-3 standard. There is no significant benefit provided by the analysis of the blast-induced ground vibrations due to its short, transient nature. The principal benefit of the improved localised approach lies in its ability to identify multiple PPV-dominant frequency estimates which could cause structural damage, particularly if there are numerous high-level events within the vibration record.

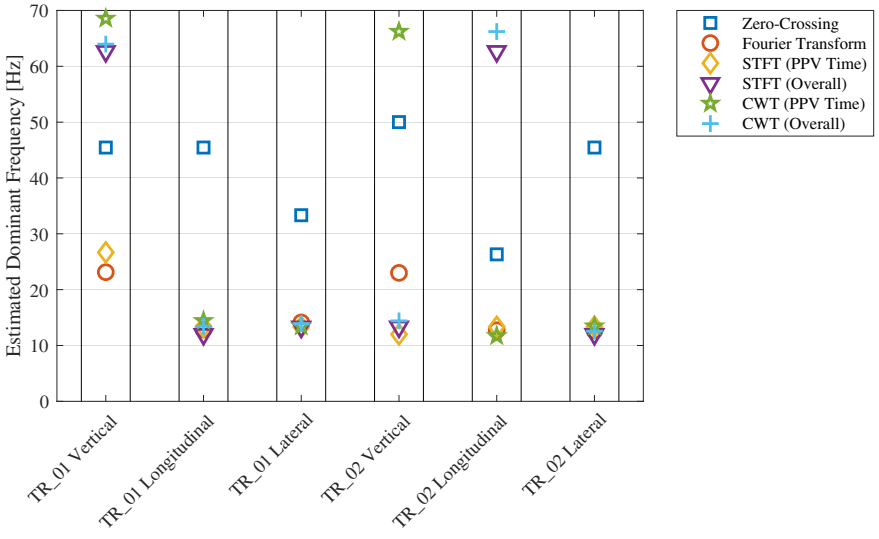

Fig. 17. Comparison of the dominant frequency estimates of the various approaches for all three components of the two train-induced ground vibrations.

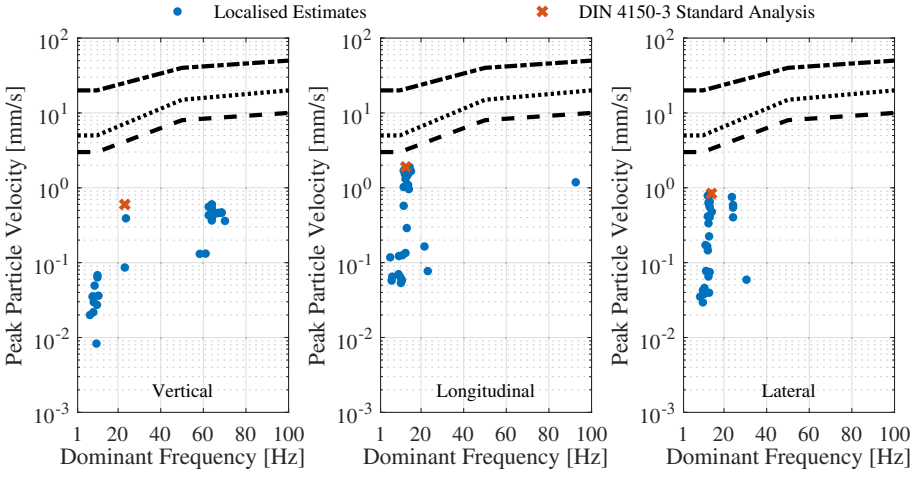

Fig. 18. Analysis of the train-induced tri-axial ground vibrations of record TR_01 using the CWT to compute localised estimates ($T_w = 0.5$ s) of the PPV and dominant frequency, presented on the DIN 4150-3 Z-Curve. Note that the vertical scale is logarithmic.

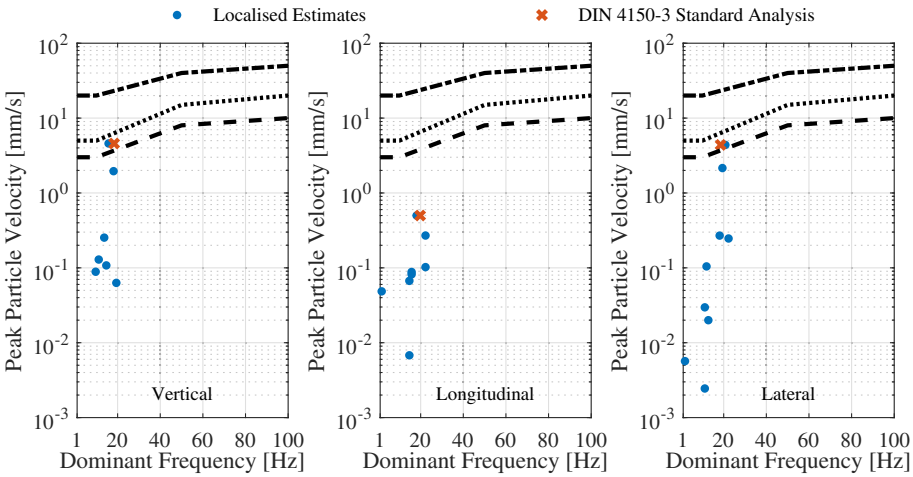

Fig. 19. Analysis of the truck-induced tri-axial ground vibrations of record RV_01 using the CWT to compute localised estimates ($T_w = 0.5$ s) of the PPV and dominant frequency, presented on the DIN 4150-3 Z-Curve. Note that the vertical scale is logarithmic.

5. Discussion and conclusions

Man-made ground vibrations in urban areas can cause issues to not only residents but also structures in the built environment. Many countries around the world have similar analysis monitoring procedures for ground vibrations to ensure they are within acceptable limits. These standards set out threshold values for both the PPV and the dominant frequency of the measured ground vibrations. There are, however, two limitations which need to be addressed. The first issue is the lack of clarity surrounding the most suitable approach for estimating the dominant frequency of the ground vibrations. The second issue is the lack of localised (in time) information provided by the standard analysis approaches.

The first part of this study presented a comparative evaluation to investigate various methods for estimating the dominant frequency. The standard analysis methods (zero-crossing, Fourier transform) were investigated, along with the use of the STFT and CWT to compute the time-frequency distributions to calculate the dominant frequency (at the time of the PPV, and from the overall distribution). Three different types of tri-axial ground vibrations due to man-made sources were each investigated using the various analysis techniques. The dominant frequency estimates of the blast-induced ground vibration records were all fairly consistent, with the exception of some isolated estimates, and all estimates using the zero-crossing approach. The train- and truck-induced ground vibrations both showed significant variation in the estimates between the methods. The zero-crossing method, which the various standards have advised against its use for complex waveforms, is considerably inaccurate and should not be used, even for simple waveforms.

Having compared the different methods, a new localised approach using the computed time-frequency distribution of the ground vibrations was described and demonstrated. The analysis of the train-induced ground vibrations resulted in the most variable estimates of the dominant frequency between the methods, due to the repeated loads induced by the passage of multiple axles. In cases such as this where the ground vibrations can last for a significant duration, the improved localised approach is more suitable. The approach used the CWT to first obtain the time-frequency distribution, and then for each section in time determined the 'localised' PPV and dominant frequency. The obtained estimates are then plotted on the DIN 4150-3 Z-Curve, and evaluated to determine if any events surpass the threshold levels for structural damage.

The example analysis using the new localised approach (involving time-frequency analysis and a moving window to obtain localised estimates of the PPV and dominant frequency), showed that the approach is able to be used with minimal difficulty to provide a far more detailed analysis. While the localised approach is not useful for single transient events, the true benefit is evident when there are a series of repeated

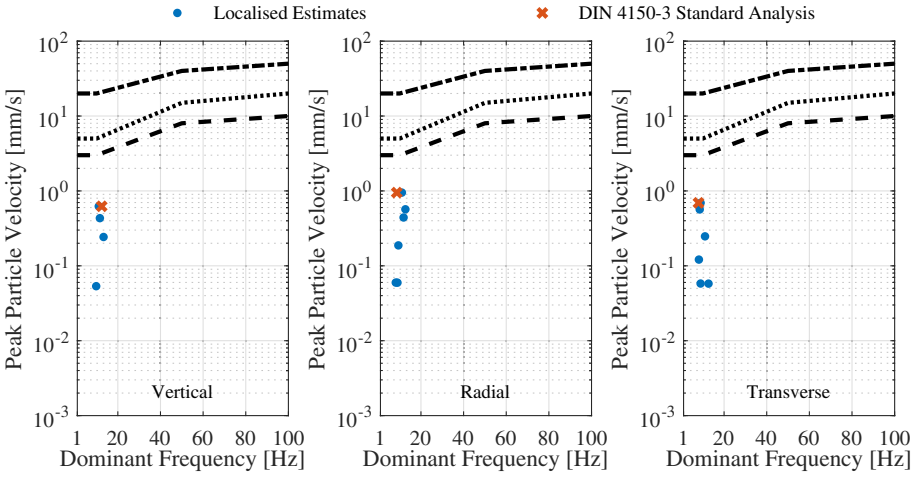

Fig. 20. Analysis of the blast-induced tri-axial ground vibrations of record BL_01 using the CWT to compute localised estimates ($T_w = 0.5$ s) of the PPV and dominant frequency, presented on the DIN 4150-3 Z-Curve. Note that the vertical scale is logarithmic.

loads induced into the ground. The improved approach is able to identify multiple events, many of which would not have been identified using the standard analysis.

Acknowledgements

The authors would like to thank Mr Vincent Van Overbeke and Mr Pierre Van Landschoot from Sagrex Quenast Belgium for providing the blast-induced ground vibration measurements.

Funding acknowledgement

This research was supported by the Fédération Wallonie-Bruxelles (Belgium) (14/19 UMONS 1) under the 2014 funding scheme "Concerted Research Actions" at the University of Mons.

References

Ainalis, D., Rouillard, V., Sek, M., 2015. On-the-road measurements to establish the dynamic characteristics of transport vehicles. Packag. Technol. Sci. 28, 657–671.
Ainalis, D., Ducarne, L., Kaufmann, O., Tshibangu, J.-P., Verlinden, O., Kouroussis, G., 2017a. Improved blast vibration analysis using the wavelet transform. 24th International Congress on Sound and Vibration, London.
Ainalis, D., Kaufmann, O., Tshibangu, J.-P., Verlinden, O., Kouroussis, G., 2017b. Modelling the source of blasting for the numerical simulation of blast-induced ground vibrations: a review. Rock Mech. Rock. Eng. 50, 171–193.
Anon, 1983. OSM Blasting Performance Standards - 30 Code of Federal Regulations. Office of Surface Mining Reclamation and Enforcement, Pittsburgh.
Anon, 1993. BS 7385-1: Evaluation and Measurement for Vibration in Buildings - Part 1: Guide for Measurement of Vibrations and Evaluation of Their Effects on Buildings. British Standards Institution, Milton Keynes.
Anon, 1999. DIN 4150-3: Vibrations in Buildings, Part 3: Effects on Structures. Beuth Verlag, Berlin.
Anon, 2006. AS 2187.2-2006: Explosives - Storage and Use - Part 2: Use of Explosives. Standards Australia, Sydney.
Anon, 2010. ISO 4866: Mechanical Vibration and Shock - Vibration of Fixed Structures - Guidelines for the Measurement of Vibrations and Evaluation of their Effects on Structures. International Organisation for Standardisation, Geneva, Switzerland.
Auersch, L., Said, S., 2010. Attenuation of ground vibrations due to different technical sources. Earthq. Eng. Eng. Vib. 9, 337–344.
Carels, P., Ophalffens, K., Vogiatzis, K., 2012. Noise and vibration evaluation of a floating slab in direct fixation turnouts in Haidari & Anthoupoli extentions of Athens metro lines 2 & 3 [Valutazione del rumore indotto e delle vibrazioni delle piattaforme flottanti negli scambi con fissaggio diretto posti lungo le estensioni "Haidari & Anthoupoli" delle linee 2 e 3 della metropolitana di Atene]. Ingegneria Ferroviaria 67, 533–553.
Cohen, L., 1995. Time-Frequency Analysis. vol. 778. Prentice Hall, New Jersey.
Connolly, D.P., Kouroussis, G., Laghrouche, O., Ho, C.L., Forde, M.C., 2015. Benchmarking railway vibrations – track, vehicle, ground and building effects. Constr. Build. Mater. 92, 64–81.
Connolly, D.P., Marecki, G.P., Kouroussis, G., Thalassinakis, I., Woodward, P.K., 2016. The growth of railway ground vibration problems—a review. Sci. Total Environ. 568, 1276–1282.
Ducarne, L., Ainalis, D., Kouroussis, G., 2017. Ground vibration generated by the passing of a truck on a speed bump. 6th International Conference on Computational Methods in Structural Dynamics and Earthquake Engineering, Rhodes.
Hunaidi, O., Guan, W., Nicks, J., 2000. Building vibrations and dynamic pavement loads induced by transit buses. Soil Dyn. Earthq. Eng. 19, 435–453.
Kim, D.-S., Lee, J.-S., 2000. Propagation and attenuation characteristics of various ground vibrations. Soil Dyn. Earthq. Eng. 19, 115–126.
Kouroussis, G., Conti, C., Verlinden, O., 2013. Experimental study of ground vibrations induced by Brussels IC/IR trains in their neighbourhood. Mech. Ind. 14, 99–105.
Kouroussis, G., Connolly, D.P., Verlinden, O., 2014. Railway-induced ground vibrations–a review of vehicle effects. Int. J. Rail Transp. 2, 69–110.
Kouroussis, G., Connolly, D.P., Alexandrou, G., Vogiatzis, K., 2015. Railway ground vibrations induced by wheel and rail singular defects. Veh. Syst. Dyn. 53, 1500–1519.
Kouroussis, G., Florentin, J., Verlinden, O., 2016. Ground vibrations induced by InterCity/InterRegion trains: a numerical prediction based on the multibody/finite element modeling approach. J. Vib. Control. 22, 4192–4210.
Kouroussis, G., Ducarne, L., Ainalis, D., 2017. Numerical modelling of the ground-borne vibrations generated by truck-road interaction. 24th International Congress on Sound and Vibration, London.
Mallat, S., 2008. A Wavelet Tour of Signal Processing: The Sparse Way. Academic Press.
Randall, R.B., 2011. Vibration-based Condition Monitoring: Industrial, Aerospace and Automotive Applications. John Wiley & Sons.
Sadowsky, J., 1996. Investigation of signal characteristics using the continuous wavelet transform. J. Hopkins APL Tech. Dig. 17, 258–269.
Siskind, D., Stagg, M., Kopp, J., Dowding, C.H., 1980. Structure Response and Damage Produced by Ground Vibration From Surface Mine Blasting. United States Bureau of Mines, New York.
Srbulov, M., 2008. Geotechnical Earthquake Engineering: Simplified Analyses With Case Studies and Examples. Springer, Berlin, Germany.
Staszewski, W., Giacomin, J., 1997. Application of the wavelet based FRFs to the analysis of nonstationary vehicle data. Proceedings-SPIE the International Society for Optical Engineering. SPIE International Society for Optical, pp. 425–431.
Vogiatzis, K., 2013. Environmental noise and vibration monitoring and assessment of major road transportation networks: the case of Elefsina (Athens)–Korinthos Motorway (2008–2011). Int. J. Sustain. Dev. Plan. 8, 173–185.